Progress In Electromagnetics Research, Vol. 129, 125–141, 2012

FOURTH STOKES PARAMETER IN POLARIMETRIC PASSIVE REMOTE SENSING FROM TWO-LAYER ROUGH SURFACES

P. Xu[1, 2, *], L. Tsang[3], and K.-S. Chen[4]

[1]School of Electronic Information, Wuhan University, China

[2]State Key Laboratory of Information Engineering in Surveying, Mapping and Remote Sensing, Wuhan University, Wuhan 430072, China

[3]Department of Electrical Engineering, University of Washington, Seattle, WA 98195, USA

[4]Center for Space and Remote Sensing, National Central University, Chung-Li 32054, Taiwan

Abstract—It has been demonstrated in previously published results that large fourth Stokes parameter may be generated from a rough surface over multi-layered media, where only the top interface is rough while the others are all flat boundaries. In this paper, we consider the four Stokes parameters in microwave emission from a two-layer rough surface. In this case, there are two rough boundaries. The rough surfaces vary in one horizontal direction so that the azimuthal asymmetry exists in the 3-D problem. Periodic boundary conditions were assumed. The results are compared with the previously published results from a rough surface over multi-layered media. It is shown that the "two-layer" periodic rough surfaces can reduce the vertical and horizontal brightness temperatures remarkably; the interactions between the two rough surfaces also enhance the third and fourth Stokes parameters, which disappear in new structure for the large dips in the vertical and horizontal brightness temperatures presented in the former Sastrugi structure. In particular, the fourth Stokes parameter can be larger than that in previous layered structure. In addition, for the case of sinusoidal rough surface without large slope with snow's permittivities, the top boundary rough only layered structure cannot support the large third and fourth Stokes parameters any longer while

Received 2 April 2012, Accepted 29 May 2012, Scheduled 15 June 2012

* Corresponding author: Peng Xu (pxu@whu.edu.cn).

the two-layer rough surface structure can do still up to $-34\,\mathrm{K}$ and $15\,\mathrm{K}$, respectively. It is also found that the reason resulting in the large fourth Stokes parameter is caused by relative magnitude of permittivities of the two layers, all cases with large fourth Stokes parameter should satisfy the upper layer's permittivity larger than the lower one due to total internal reflection from the lower layer.

1. INTRODUCTION

In passive polarimetric microwave remote sensing, the first two components of the full polarimetric Stokes vectors, representing the vertical and horizontal polarizations, define electromagnetic radiation; the third and fourth components, representing the real and imaginary parts of the cross correlation of the first two components, respectively, are mostly related to the asymmetric structure of the surface roughness [1]. Thus the third and fourth Stokes parameters contain information of the azimuthal structure, and they are usually used for inversion of wind speed and direction over ocean and snow surfaces, even for remote sensing of target recognition, to name a few.

Usually the fourth Stokes parameter V is small in measurements and of the order $\pm 2.5\,\mathrm{K}$. In the past theoretical works have also indicated that the third Stokes parameter U may become large but not for the fourth Stokes parameter V [1–3]. However, it is observed that the fourth Stokes parameter can be appreciable and is up to $\pm 12\,\mathrm{K}$ over Greenland which is a surprise as never before [4]. In 2008. we proposed a model of a Sastrugi surface over layered media [5], values of V can be as large as $-20\,\mathrm{K} \sim 10\,\mathrm{K}$ due to total internal reflections from lower layers if given the upper layer's permittivity ε_1 larger than the lower ε_2. In this previous case, only the top boundary is rough with multi-layered media down below. The Sastrugi surface is produced due to strong wind in Greenland, and the layered structure is possible because the densities of snow change as snow accumulates, which gives permittivity between 1.3 and 1.8. Thus it is possible for a layer of permittivity 1.8 to lie above a layer of permittivity 1.3 creating the total internal reflection.

Most natural surfaces are generally not smooth but rough. In this paper, different from the previous model in Ref. [5], where only the top interface is rough while the others are all flat faces, a two-layer rough surface is studied to simulate the four Stokes parameters in passive microwave remote sensing. Earlier, Petit [6] used this type of structure to study the grating efficiency. Kuo and Moghaddam [7] used the extended boundary condition method to exam the scattering only for multilayer random rough surfaces in the context with active remote sensing. Johnson et al. [3] used this model to study passive polarimetry of wind direction over the ocean. However, their works were restricted to roughness small in height and slope compared with those used in this paper. Also in Johnson's work, the permittivity of the fiberglass layer ε_1 is smaller than ε_2 of the seawater, thus their results did not exhibit the large fourth Stokes parameter. In this paper, we use numerical solution of Maxwell equations to study the problem of polarimetric passive microwave remote sensing of a two-layer rough surface, with the upper layer's permittivity ε_1 larger than ε_2 of the lower. Our results show that the interactions between the rough surface scattering and reflection by layering can give large fourth Stokes parameter, and the large dips in the vertical and horizontal polarizations presented in the previous Sastrugi structure [5], are not seen in the two-layer Sastrugi structure. Moreover, even for the case of sinusoidal rough surface with snow's permittivities without large surface slopes, the considered structure can still support large third and fourth Stokes parameters up to -34 K and 15 K, respectively. In Section 2, We follow the surface integral equation formulations in Ref. [3] to treat the 3-D scattering, emission and absorption of a two-layer rough surface. More accurate and efficient solution is obtained by using rooftop basis function and Galerkin's method in moment method. In Section 3, numerical results are illustrated for polarimetric passive microwave remote sensing and compared with the previous model of a single rough surface. Results of all four Stokes parameters are shown for sinusoid and Sastrugi of the top surface. Finally conclusion is drawn to show that the considered structure is more reasonable to interpret the observed large values of the fourth Stokes parameter.

2. FORMULATIONS

Consider a plane wave incident upon a two-layer periodic surface with height profile $z = f_1(x + P)$ and $z = f_2(x + P)$ with f_1 and f_2 representing the top and the bottom surfaces, respectively, and P denoting the period of the surface in the $\hat{x}$ direction as shown in Fig. 1. The second rough surface is placed at $z = -d$ below the top one. The region zero above the top surface is air, the other two layers are with permittivities of ε_1 and ε_2, respectively. The incident electromagnetic fields are given by

$$\begin{cases} \bar{E}_i = E_{vi}\hat{v}_i + E_{hi}\hat{h}_i & \text{(1a)} \\ \eta_0\bar{H}_i = E_{vi}\hat{h}_i - E_{hi}\hat{v}_i & \text{(1b)} \end{cases}$$

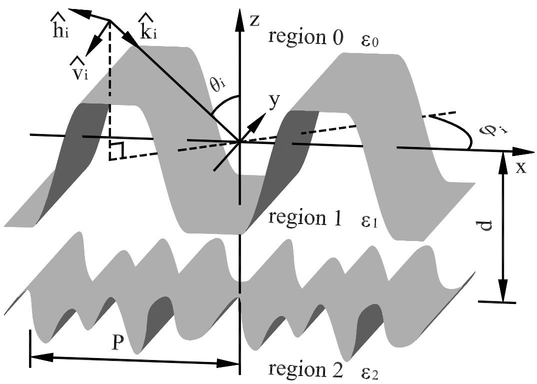

Figure 1. Geometry of a two-layer grating structure. The top surface is depicted as a periodic Sastrugi profile, and the bottom one as a periodic random rough surface, which is random within its period.

where

$$\begin{cases} E_{hi} = \cos\alpha \exp\left(ik\bar{r}\cdot\hat{k}_i\right)\exp(-i\beta) & \text{(2a)} \\ E_{vi} = \sin\alpha \exp\left(ik\bar{r}\cdot\hat{k}_i\right) & \text{(2b)} \end{cases}$$

$$\begin{cases} \hat{k}_i = \sin\theta_i\cos\varphi_i\hat{x} + \sin\theta_i\sin\varphi_i\hat{y} - \cos\theta_i\hat{z} & \text{(3a)} \\ \hat{h}_i = -\sin\varphi_i\hat{x} + \cos\varphi_i\hat{y} & \text{(3b)} \\ \hat{v}_i = -\cos\theta_i\cos\varphi_i\hat{x} - \cos\theta_i\sin\varphi_i\hat{y} - \sin\theta_i\hat{z} & \text{(3c)} \end{cases}$$

With the incident directions given above, $k_{ix} = k\sin\theta_i\cos\varphi_i$; $k_{iy} = k\sin\theta_i\sin\varphi_i$; $k_{iz} = -k\cos\theta_i$. The parameters α and β are used to characterize the polarizations.

Following Ref. [3], the surface integral equations based on Maxwell's equations with the boundary conditions can be gotten in region 0, 1, and 2, respectively.

$$\frac{1}{2}\psi_0(x') - \fint_{P(s_1)} ds\psi_0(x)\hat{n}\cdot\nabla_t g_{0P} + \int_{P(s_1)} dsg_{0P}\chi_0(x)$$
$$= E_{iyw}\left(x', f(x')\right) \tag{4a}$$

$$\frac{1}{2}\eta_0\phi_0(x') - \fint_{P(s_1)} ds\eta_0\phi_0(x)\hat{n}\cdot\nabla_t g_{0P} + \int_{P(s_1)} dsg_{0P}\eta_0\xi_0(x)$$
$$= \eta_0 H_{iyw}\left(x', f(x')\right) \tag{4b}$$

$$-\frac{1}{2}\psi_0(x') - \fint_{P(s_1)} ds\psi_0(x)\hat{n}\cdot\nabla_t g_{1P}$$
$$+a_1\int_{P(s_1)} dsg_{1P}\chi_0(x) + c_1\int_{P(s_1)} g_{1P}d\eta_0\phi_0(x)$$
$$-\left[\frac{1}{2}\psi_1(x') - \fint_{P(s_2)} ds\psi_1(x)\hat{n}\cdot\nabla_t g_{1P} + \int_{P(s_2)} dsg_{1P}\chi_1(x)\right] = 0 \tag{4c}$$
$$-\frac{1}{2}\eta_0\phi_0(x') - \fint_{P(s_1)} ds\eta_0\phi_0(x)\hat{n}\cdot\nabla_t g_{1P}$$
$$+a_1\tau_1\int_{P(s_1)} dsg_{1P}\eta_0\xi_0(x) - c_1\tau_1\int_{P(s_1)} g_{1P}d\psi_0(x)$$
$$-\left[\frac{1}{2}\eta_0\phi_1(x') - \fint_{P(s_2)} ds\eta_0\phi_1(x)\hat{n}\cdot\nabla_t g_{1P} + \int_{P(s_2)} dsg_{1P}\eta_0\xi_1(x)\right] = 0 \tag{4d}$$
$$-\frac{1}{2}\psi_1(x') - \fint_{P(s_2)} ds\psi_1(x)\hat{n}\cdot\nabla_t g_{2P} + a_2\int_{P(s_2)} dsg_{2P}\chi_1(x)$$
$$+c_2\int_{P(s_2)} g_{2P}d\eta_1\phi_1(x) = 0 \tag{4e}$$
$$-\frac{1}{2}\eta_1\phi_1(x') - \fint_{P(s_2)} ds\eta_1\phi_1(x)\hat{n}\cdot\nabla_t g_{2P} + a_2\tau_2\int_{P(s_2)} dsg_{2P}\eta_1\xi_1(x)$$
$$-c_2\tau_2\int_{P(s_2)} g_{2P}d\psi_1(x) = 0 \tag{4f}$$

where $\fint$ denotes a principle value of integral, and g_{jP} is 2-D periodic Green function in region j and is fast computed by method of Veysoglu et al. [1].

The surface unknowns are the $\hat{y}$ components of surface electric and magnetic fields and their normal derivatives on the top surface in region 0 and on the bottom surface in region 1, respectively.

$$\begin{cases} \psi_0(x) = E_{0yw}(s_1) & \text{(5a)} \\ \eta_0\phi_0(x) = \eta_0 H_{0yw}(s_1) & \text{(5b)} \\ \chi_0(x) = \hat{n}\cdot\nabla_t E_{0yw}(s_1) & \text{(5c)} \\ \eta_0\xi_0(x) = \eta_0\hat{n}\cdot\nabla_t H_{0yw}(s_1) & \text{(5d)} \end{cases}$$

$$\begin{cases} \psi_1(x) = E_{1yw}(s_2) & \text{(6a)} \\ \eta_1\phi_1(x) = \eta_1 H_{1yw}(s_2) & \text{(6b)} \\ \chi_1(x) = \hat{n}\cdot\nabla_t E_{1yw}(s_2) & \text{(6c)} \\ \eta_1\xi_1(x) = \eta_1\hat{n}\cdot\nabla_t H_{1yw}(s_2) & \text{(6d)} \end{cases}$$

where η_0 and η_1 are wave impedances, respectively, in region 0 and 1, and $H_{jyw} \exp(ik_{iy}y) = H_{jy}$, $E_{jyw} \exp(ik_{iy}y) = E_{jy}$ for $j = i$ (incident), 0 and 1.

And

$$\begin{cases} \tau_j = \dfrac{\varepsilon_j}{\varepsilon_{j-1}} & \text{(7a)} \\ a_j = \dfrac{\varepsilon_{j-1} k_{jt}^2}{\varepsilon_j k_{(j-1)t}^2} = \dfrac{k_{jt}^2}{\tau_j k_{(j-1)t}^2} & \text{(7b)} \\ c_j = \dfrac{\varepsilon_{(j-1)} k_{iy}}{\varepsilon_j k_{(j-1)}} \left(\dfrac{k_{jt}^2}{k_{(j-1)t}^2} - 1 \right) & \text{(7c)} \end{cases}$$

for $j = 1$ and 2; and

$$\begin{cases} k_{jt}^2 = k_j^2 - k_{iy}^2 & \text{(8a)} \\ \nabla_t = \hat{x}\dfrac{\partial}{\partial x} + \hat{z}\dfrac{\partial}{\partial z} & \text{(8b)} \end{cases}$$

for $j = 0$, 1, 2.

The surface is discretized such that each segment has equal surface length of $\Delta\ell = \Delta x_n \sqrt{1 + f_n'^2}$. Note that due to large slope of the rough surface, the points are not equally spaced on the x axis. Using a set of N rooftop basis functions and Galerkin's method, result in a following matrix equation of dimensions $8N \times 8N$.

$$\left[\begin{matrix} a_1\bar{\bar{A}}^{(1)}_{(s_1',s_1)} & \bar{\bar{B}}^{(1)}_{(s_1',s_1)} & c_1\bar{\bar{C}}^{(1)}_{(s_1',s_1)} & \bar{\bar{0}} & -\bar{\bar{A}}^{(1)}_{(s_1',s_2)} \\ \bar{\bar{A}}^{(0)}_{(s_1',s_1)} & \bar{\bar{B}}^{(0)}_{(s_1',s_1)} & \bar{\bar{0}} & \bar{\bar{0}} & \bar{\bar{0}} \\ \bar{\bar{0}} & \bar{\bar{0}} & \bar{\bar{B}}^{(0)}_{(s_1',s_1)} & \bar{\bar{A}}^{(0)}_{(s_1',s_1)} & \bar{\bar{0}} \\ \bar{\bar{0}} & -\tau_1 c_1\bar{\bar{C}}^{(1)}_{(s_1',s_1)} & \bar{\bar{B}}^{(1)}_{(s_1',s_1)} & \tau_1 a_1\bar{\bar{A}}^{(1)}_{(s_1',s_1)} & \bar{\bar{0}} \\ \bar{\bar{0}} & \bar{\bar{0}} & \bar{\bar{0}} & \bar{\bar{0}} & a_2\bar{\bar{A}}^{(2)}_{(s_2',s_2)} \\ a_1\bar{\bar{A}}^{(1)}_{(s_2',s_1)} & \bar{\bar{B}}^{(1)}_{(s_2',s_1)} & c_1\bar{\bar{C}}^{(1)}_{(s_2',s_1)} & \bar{\bar{0}} & -\bar{\bar{A}}^{(1)}_{(s_2',s_2)} \\ \bar{\bar{0}} & -\tau_1 c_1\bar{\bar{C}}^{(1)}_{(s_2',s_1)} & \bar{\bar{B}}^{(1)}_{(s_2',s_1)} & \tau_1 a_1\bar{\bar{A}}^{(1)}_{(s_2',s_1)} & \bar{\bar{0}} \\ \bar{\bar{0}} & \bar{\bar{0}} & \bar{\bar{0}} & \bar{\bar{0}} & \bar{\bar{0}} \end{matrix}\right.$$

$$\left.\begin{matrix} -\bar{\bar{B}}^{(1)}_{(s'_1,s_2)} & \bar{\bar{0}} & \bar{\bar{0}} \\ \bar{\bar{0}} & \bar{\bar{0}} & \bar{\bar{0}} \\ \bar{\bar{0}} & \bar{\bar{0}} & \bar{\bar{0}} \\ \bar{\bar{0}} & -\sqrt{\tau_1}\bar{\bar{B}}^{(1)}_{(s'_1,s_2)} & -\sqrt{\tau_1}\bar{\bar{A}}^{(1)}_{(s'_1,s_2)} \\ \bar{\bar{B}}^{(2)}_{(s'_2,s_2)} & c_2\bar{\bar{C}}^{(2)}_{(s'_2,s_2)} & \bar{\bar{0}} \\ -\bar{\bar{B}}^{(1)}_{(s'_2,s_2)} & \bar{\bar{0}} & \bar{\bar{0}} \\ \bar{\bar{0}} & -\sqrt{\tau_1}\bar{\bar{B}}^{(1)}_{(s'_2,s_2)} & -\sqrt{\tau_1}\bar{\bar{A}}^{(1)}_{(s'_2,s_2)} \\ -\tau_2 c_2\bar{\bar{C}}^{(2)}_{(s'_2,s_2)} & \bar{\bar{B}}^{(2)}_{(s'_2,s_2)} & \tau_2 a_2\bar{\bar{A}}^{(2)}_{(s'_2,s_2)} \end{matrix}\right] \begin{bmatrix} \bar{\chi}_0 \\ \bar{\psi}_0 \\ \eta_0\bar{\phi}_0 \\ \eta_0\bar{\xi}_0 \\ \bar{\chi}_1 \\ \bar{\psi}_1 \\ \eta_1\bar{\phi}_1 \\ \eta_1\bar{\xi}_1 \end{bmatrix} = \begin{bmatrix} \bar{0} \\ \bar{E}_{iyw} \\ \eta_0\bar{H}_{iyw} \\ \bar{0} \\ \bar{0} \\ \bar{0} \\ \bar{0} \\ \bar{0} \end{bmatrix} \tag{9}$$

where

$$\begin{cases} A^{(j=0,1,2)}_{(s',s)mn} = \int_{P(s')} dx' F_m\left(x'\right) \int_{P(s)} F_n\left(x\right) g_{jP}\left(s',s\right) ds & \text{(10a)} \\ B^{(0)}_{(s'_1,s_1)mn} = \frac{1}{2}\int_{P(s'_1)} dx' F_m\left(x'\right) F_n\left(x'\right) & \\ -\int_{P(s'_1)} dx' F_m\left(x'\right) -\!\!\!\!\!\!\int_{P(s_1)} F_n\left(x\right) \hat{n}\cdot\nabla_t g_{0P}\left(s'_1,s_1\right) ds & \text{(10b)} \\ B^{(1)}_{(s'_1,s_1)mn} = -\frac{1}{2}\int_{P(s'_1)} dx' F_m\left(x'\right) F_n\left(x'\right) & \\ -\int_{P(s'_1)} dx' F_m\left(x'\right) -\!\!\!\!\!\!\int_{P(s_1)} F_n\left(x\right) \hat{n}\cdot\nabla_t g_{1P}\left(s'_1,s_1\right) ds & \text{(10c)} \\ B^{(1),i\neq j}_{(s'_i,s_j)mn} = -\int_{P(s'_i)} dx' F_m(x') \int_{P(s_j)} F_n(x)\hat{n}\cdot\nabla_t g_{1P}\left(s'_i,s_j\right) ds & \text{(10d)} \\ B^{(1)}_{(s'_2,s_2)mn} = \frac{1}{2}\int_{P(s'_2)} dx' F_m\left(x'\right) F_n\left(x'\right) & \\ -\int_{P(s'_2)} dx' F_m\left(x'\right) -\!\!\!\!\!\!\int_{P(s_2)} F_n\left(x\right) \hat{n}\cdot\nabla_t g_{1P}\left(s'_2,s_2\right) ds & \text{(10e)} \\ B^{(2)}_{(s'_2,s_2)mn} = -\frac{1}{2}\int_{P(s'_2)} dx' F_m\left(x'\right) F_n\left(x'\right) & \\ -\int_{P(s'_2)} dx' F_m\left(x'\right) -\!\!\!\!\!\!\int_{P(s_2)} F_n\left(x\right) \hat{n}\cdot\nabla_t g_{2P}\left(s'_2,s_2\right) ds & \text{(10f)} \\ C^{(j=1,2)}_{(s',s)mn} = \int_{P(s')} dx' F_m\left(x'\right) \int_{P(s)} \frac{dF_n\left(x\right)}{dx} g_{jP}\left(s',s\right) dx & \text{(10g)} \end{cases}$$

where F is the rooftop basis function.

Emissivity is equal to absorptivity. After the surface fields are determined, absorptivity and reflectivity can be calculated by

$$\begin{cases} a(\theta_i,\varphi_i) = +\dfrac{k}{k_{0t}^2 P\cos\theta_i}\operatorname{Im}\displaystyle\int_{P(s_1)} dx\left[\psi_0(x)\chi_0^*(x) - \eta_0^2\xi_0(x)\phi_0^*(x)\right] & \text{(11a)} \\ r(\theta_i,\varphi_i) = -\dfrac{k}{k_{0t}^2 P\cos\theta_i}\operatorname{Im}\displaystyle\int_{P(s_1)} dx\left[\psi_0^s(x)\chi_0^{s*}(x) - \eta_0^2\xi_0^s(x)\phi_0^{s*}(x)\right] & \text{(11b)} \end{cases}$$

where

$$\begin{cases} \psi_0^s(x) = \psi_0(x) - E_{iyw}(s_1) & \text{(12a)} \\ \phi_0^{s*}(x) = \phi_0^*(x) - H_{iyw}^*(s_1) & \text{(12b)} \\ \chi_0^{s*}(x) = \chi_0^*(x) - \hat{n}\cdot\nabla_t E_{iyw}^*(s_1) & \text{(12c)} \\ \xi_0^s(x) = \xi_0(x) - \hat{n}\cdot\nabla_t H_{iyw}(s_1) & \text{(12d)} \end{cases}$$

In passive remote sensing, the energy conservation test is by showing numerically that $a(\theta_i,\varphi_i) + r(\theta_i,\varphi_i) = 1$. All energy tests in this paper satisfy energy conservation to less than 1%, which can be improved further by dense discretization.

For polarizations, let $\gamma = v,\ h,\ +45°,\ -45°,\ \mathrm{LC},\ \mathrm{RC}$ be vertical, horizontal, +45° linear, −45° linear, left-hand circular and right-hand circular polarizations respectively. The brightness temperatures are related to the emissivities by

$$T_\gamma(\theta_i,\varphi_i) = e_\gamma(\theta_i,\varphi_i)\,T_0 \tag{13}$$

where T_0 is the physical temperature. The four Stokes parameters are T_v, T_h, $U = T_{+45°} - T_{-45°}$, and $V = T_{LC} - T_{RC}$. The third and fourth Stokes parameters for azimuthal asymmetric structure can be nonzero due to the differences of the incident electric fields between ±45°linear polarizations, and between left-hand circular, and right-hand circular polarizations.

$$\begin{cases} \bar{E}_{+45°} = -\exp\left(ik\bar{r}\cdot\hat{k}_i\right) & \\ /\sqrt{2}\left[\hat{x}\left(\cos\theta_i\cos\varphi_i + \sin\varphi_i\right) + \hat{y}\left(\cos\theta_i\sin\varphi_i - \cos\varphi_i\right) + \hat{z}\sin\theta_i\right] & \text{(14a)} \\ \bar{E}_{-45°} = -\exp\left(ik\bar{r}\cdot\hat{k}_i\right) & \\ /\sqrt{2}\left[\hat{x}\left(\cos\theta_i\cos\varphi_i - \sin\varphi_i\right) + \hat{y}\left(\cos\theta_i\sin\varphi_i + \cos\varphi_i\right) + \hat{z}\sin\theta_i\right] & \text{(14b)} \\ \bar{E}_{\mathrm{LC}} = -\exp\left(ik\bar{r}\cdot\hat{k}_i\right) & \\ /\sqrt{2}\left[\hat{x}(\cos\theta_i\cos\varphi_i - i\sin\varphi_i) + \hat{y}(\cos\theta_i\sin\varphi_i + i\cos\varphi_i) + \hat{z}\sin\theta_i\right] & \text{(14c)} \\ \bar{E}_{\mathrm{RC}} = -\exp\left(ik\bar{r}\cdot\hat{k}_i\right) & \\ /\sqrt{2}\left[\hat{x}(\cos\theta_i\cos\varphi_i + i\sin\varphi_i) + \hat{y}(\cos\theta_i\sin\varphi_i - i\cos\varphi_i) + \hat{z}\sin\theta_i\right] & \text{(14d)} \end{cases}$$

Please note that the amplitudes of x and y components are different between $\pm 45°$linear polarizations if given $\varphi_i \neq 0$ or $90°$, while they are equal for amplitudes and different only for phase angles between two circular polarizations. It means that the fourth Stokes parameter is typically smaller than the third one.

3. NUMERICAL RESULTS AND DISCUSSION

For the purpose of simulation, following Ref. [5], a sinusoidal profile $f(x) = A \sin(2\pi x/P)$, with $A = 15\,\text{cm}$ and $P = 50\,\text{cm}$ is used with the second surface at $z = -d = -16.8\,\text{cm}$. The permittivities of region 1 and 2 are $\varepsilon_1 = 6$ and $\varepsilon_2 = 2$, respectively. The frequency is 1 GHz and physical temperature is at 300 K. In Figs. 2(a) and (b), we show the dependence on azimuthal angle of all four Stokes parameters, respectively, at two fixed polar angles of $\theta = 20°$ and $70°$ for three types of structures. The dependence on polar angle at a fixed azimuthal angle of $\varphi = 45°$ is shown in Fig. 2(c).

We compared the new results of the two-layer sinusoidal surface with the case of rough surface alone which is a single rough surface over an infinite half space of $\varepsilon_1 = 6$. The other case is a single rough surface over a layered medium with $\varepsilon_1 = 6$ and $\varepsilon_2 = 2$ and the bottom interface is smooth. Comparing with results of the rough surface alone, it is shown in Fig. 2 that the presence of layered structures can reduce the vertical and horizontal brightness temperatures significantly, and produce large third and fourth Stokes parameters. The third and fourth Stokes parameters for all cases become zero at two ends of $\varphi = 0$ and $90°$ because here are no differences between $\pm 45°$ linear polarizations and between two circular polarizations as depicted in Equation (14). As evidenced at a small polar angle in Fig. 2(a), the fourth Stokes parameter for the case of the single surface alone is close to zero, while the two-layer rough surface structure can produce large fourth Stokes parameter that is comparable to that of the rough surface over a layer medium. And the vertical and horizontal brightness temperatures are larger than those of the case of the rough surface over layered medium. As shown in Fig. 2(b) at the large fixed polar angle, the presence of sinusoid-sinusoid structure give low vertical and horizontal brightness temperatures down to 101 K and 42 K, respectively, while generating larger third and fourth Stokes parameters up to $-138\,\text{K}$ and 226 K, respectively. It is also shown in Fig. 2(b4) that even a single rough surface alone can pronouncedly generate the fourth Stokes parameter up to $-25\,\text{K}$ at large polar angle. On the other hand, with increase of the polar angle from $\theta = 20°$ to $70°$, the angular curves of all four Stokes parameters become more

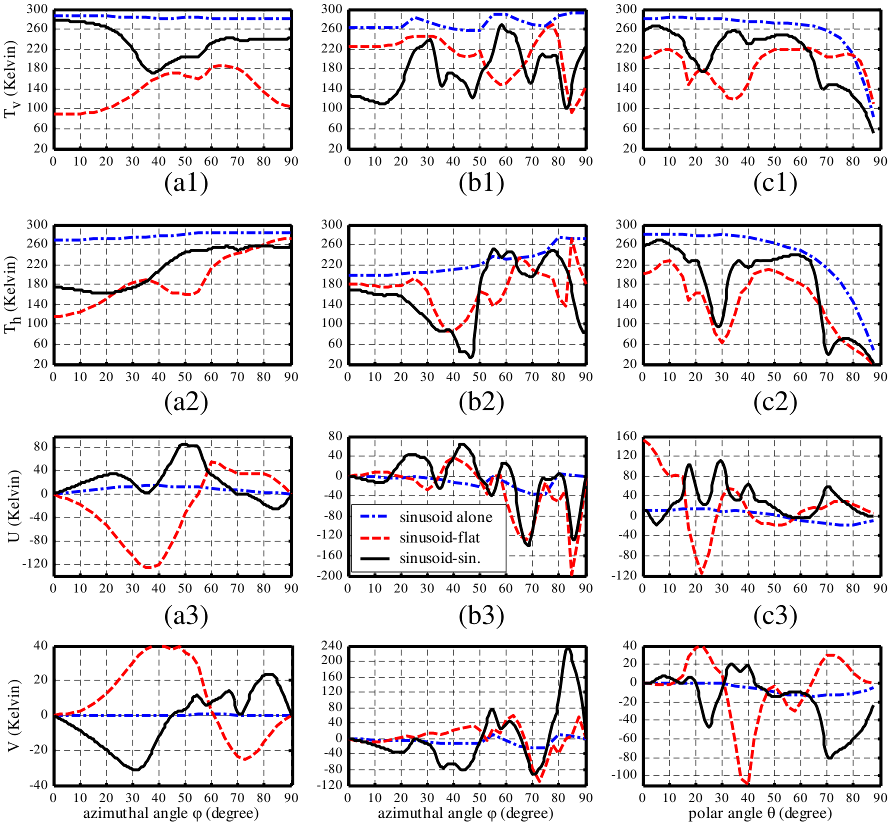

Figure 2. Comparison of four stokes parameters at frequency of 1 GHz with physics temperature $T_0 = 300\,\mathrm{K}$ among a single sinusoidal surface alone, a single sinusoid over a flat layer, and a two-layer sinusoid. Sinusoidal surface is $f(x) = 15 \sin(2\pi x/50)\,\mathrm{cm}$ with $d = 16.8\,\mathrm{cm}$, $\varepsilon_1 = 6$ and $\varepsilon_2 = 2$. (a) and (b) are plotted as a function of azimuthal angle at fixed polar angle $\theta = 20^\circ$ and $\theta = 70^\circ$, respectively, (c) as a function of polar angle at fixed azimuthal angle $\varphi = 45^\circ$. The dash-dot line is for a single sinusoid alone; the dash line is for a single sinusoid over a flat layer; and the solid line is for a two-layer sinusoid.

fluctuating, as clearly visible in comparison of Fig. 2(b) with Fig. 2(a); the vertical and horizontal brightness temperatures decrease further while the fourth Stokes parameter increases more and the third Stokes parameter basically remains the same order.

All four Stokes parameters' angular trends also become fluctuant versus polar angle at the fixed azimuthal angle of 45° for both layered structures as shown in Fig. 2(c). The polar angular behavior for the single rough surface alone is much smoother. In particular, the vertical and horizontal brightness temperatures are almost monotonic decreasing with the increase of polar angle. As the polar angle approaches to 90°, the values of all four Stokes parameters for three types of structures seem to converge at a certain point respectively. In particular, the third Stokes parameter and the fourth one converge to zero. However, as the polar angle approaches to zero, only the fourth Stokes parameter converges to zero, the third one for the case of the single sinusoidal surface over a flat layer is no longer close to zero as shown in Fig. 2(c3). It is apprehensible that the polar angular behavior of the third Stokes parameter at the end of $\theta = 0$ doesn't like the azimuthal angular behavior at the end of $\varphi = 0$. Seen from Equation (14), the incident electric fields are completely different at $\theta = 0$ between ±45° linear polarizations while those are uniform at $\varphi = 0$.

As another example, a Sastrugi-type surface [5], which has been depicted by the top surface in Fig. 1, is used for simulation. The Sastrugi surface in a period P has

$$f(x)=\begin{cases}-A\cos(4\pi x/P) & \text{for } mP \le x < (0.25+m)P \\ A & \text{for } (0.25+m)P \le x < (0.50+m)P \\ A\cos(4\pi x/P) & \text{for } (0.50+m)P \le x < (0.75+m)P \\ -A & \text{for } (0.75+m)P \le x < (1+m)P \end{cases}, \quad m=-\infty,\ldots,0,1,\ldots,\infty \tag{15}$$

The surface height was set to $A = 7.5\,\text{cm}$, the period $P = 25\,\text{cm}$, and the permittivities $\varepsilon_1 = 1.8 + i6E - 4$, $\varepsilon_2 = 1.3 + i3.3E - 4$, as in the case of snow with a small imaginary part. We consider operating frequency of 10 GHz with a polar angle $\theta = 55°$. The physical temperature was set to 250 K. As shown in Fig. 3, both layered structures significantly reduce the vertical and horizontal brightness temperatures, and generate larger third and fourth Stokes parameters in comparison with those from a single Sastrugi surface alone. In addition, there are dips around $\varphi = 56°$ down to 132 K and 113 K, respectively, in vertical and horizontal brightness temperatures for the Sastrugi-flat structure. On the contrary, the large dips in the two-layer rough structure disappear and present more peaks with fairly small fluctuations. The Sastrugi-Sastrugi structure clearly pushes the fourth Stokes up to 24 K and third Stokes down to −25 K. It seems reverse for the Sastrugi-flat structure in which the third Stokes is pushed up to 25 K, while the fourth Stokes down to a little higher to −20 K.

If the second interface is replaced by a periodic random rough surface with exponential correlation function with rms height of 1 cm

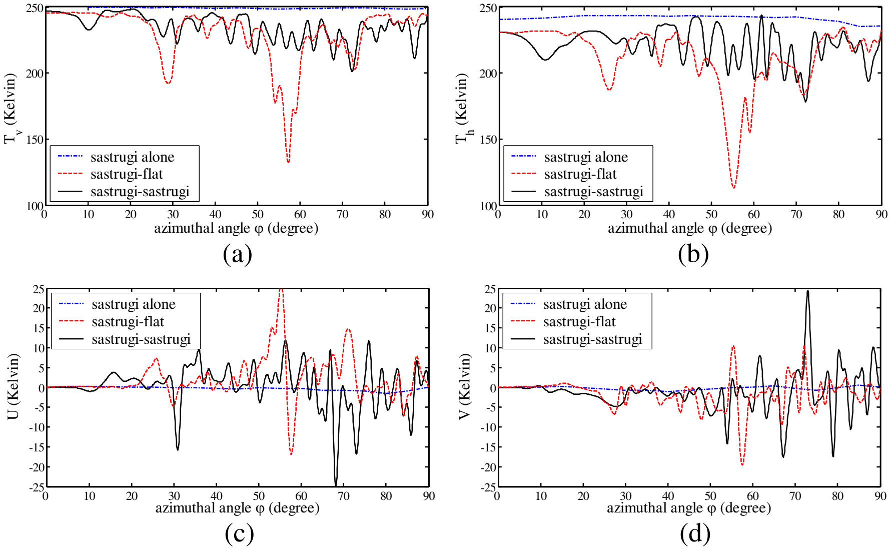

Figure 3. Comparison of four Stokes parameters versus azimuthal angle at fixed polar angle $\theta = 55°$ among a single Sastrugi surface alone, a single Sastrugi surface over a flat layer, and a two-layer Sastrugi surface with $d = 12.5\,\mathrm{cm}$, $\varepsilon_1 = 1.8 + i6E - 4$, $\varepsilon_2 = 1.3 + i3.3E - 4$. Freq $= 10\,\mathrm{GHz}$ with $T_0 = 250\,\mathrm{K}$. The dash-dot line is for a single Sastrugi surface alone; the dash line is for a single Sastrugi surface over a flat layer; and the solid line is for a two-layer Sastrugi surface. (a) Vertical brightness, (b) horizontal brightness, (c) U brightness, and (d) V brightness.

and correlation length of 10 cm, after averaging over 8 realizations, it is found that the large dips in vertical and horizontal brightness temperatures are still presented as shown in Fig. 4. And also its angular curves of the vertical and horizontal brightness temperatures are similar to those of the Sastrugi-flat structure. That means that the bottom surface does not rough enough to remove these large dips. If the top surface of the periodic Sastrugi is replaced by a random Sastrugi, which is a large scale problem and not reported in this paper, we deduce that these large dips may also be removed as the case of the periodic two-layer Sastrugi.

It is interesting now to see the effect of type of rough surface. To do so, the large sloped Sastrugi surface is replaced by a sinusoidal rough surface without large slope with the permittivities, the fixed polar angle and frequency same as those in Fig. 3. In such case, the

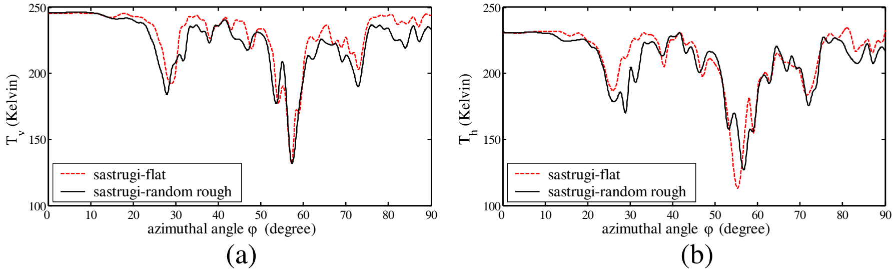

Figure 4. Comparison of vertical and horizontal brightness temperatures versus azimuthal angle at fixed polar angle $\theta = 55°$ between a single Sastrugi surface over a flat layer and a two-layer rough surface, where the top surface does not change, while the bottom interface is replaced by a periodic random exponential correlated surface with rms height 1 cm and correlation length 10 cm. Both cases are with $d = 12.5\,\text{cm}$, $\varepsilon_1 = 1.8 + i6E - 4$, $\varepsilon_2 = 1.3 + i3.3E - 4$. Freq $= 10\,\text{GHz}$ with $T_0 = 250\,\text{K}$. The dash line is for a single Sastrugi surface over a flat layer; the solid line is for a two-layer rough surface averaging over 8 realizations. (a) Vertical brightness, and (b) horizontal brightness.

sinusoid-flat structure is no longer able to generate large third and fourth Stokes parameters as shown in Fig. 5. Note that the sinusoidal surface is of the form $f(x) = 7.5\sin(2\pi x/30)$ cm with $d = 17\,\text{cm}$. It is also observed that the new two-layer rough surface structure is still able to produce the third Stokes parameter up to $-34\,\text{K}$, and the fourth Stokes parameter up to 15.9 K due to the wave of total internal reflection from the bottom rough boundary.

Generally, the $U = T_{+45°} - T_{-45°}$ can be large on a single rough surface alone once the difference between ε_0 and ε_1 is large enough, while the $V = T_{LC} - T_{RC}$ cannot be so except that both ε_1 and polar angle are simultaneously large enough. It can be seen from Equation (14) that the absolute values of x and y electric field components between $\pm 45°$ polarizations are different only if $\varphi_i \neq 0$ or $90°$, so it is easy to produce large U. However, those between left and right hand circular polarizations are equal, and only phase angles are different. That is why a single surface alone is not easy to produce large V even with a large ε_1. In two-layer cases, the total reflection may be taken place on the bottom interface if $\varepsilon_1 > \varepsilon_2$, which enhances the differences of emission even for left and right hand circular polarizations, and results in not only larger U but also larger V. As shown in Fig. 6, the roughness on the second interface enhances total

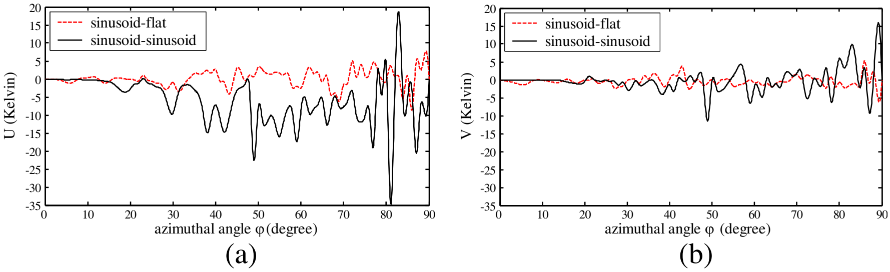

Figure 5. Comparison of the third and fourth Stokes parameters versus azimuthal angle at fixed polar angle $\theta = 55°$ between a single sinusoidal surface over a flat layer and a two-layer sinusoidal surface. $f(x) = 7.5 \sin(2\pi x/30)$ cm with $d = 17$ cm, $\varepsilon_1 = 1.8 + i6E - 4$, $\varepsilon_2 = 1.3 + i3.3E - 4$. Freq $= 10$ GHz with $T_0 = 250$ K. The dash line is for a single sinusoidal surface over a flat layer; the solid line is for a two-layer sinusoidal surface. (a) U brightness, and (b) V brightness.

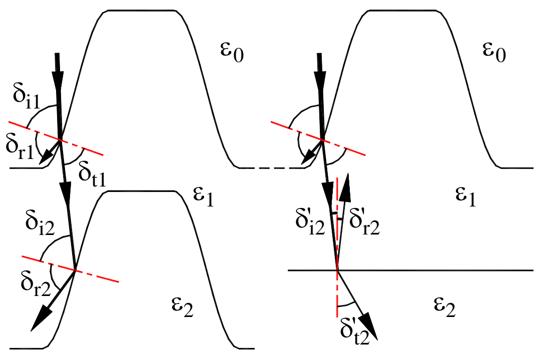

Figure 6. Comparison of total internal reflection on bottom interface between with and without large slope. If $\delta_{i2} >$ critical angle $> \delta'_{i2}$, left panel shows the total reflection while right panel shows no total reflection.

reflection than the smooth one as $\delta_{i2} >$ criticalangle $> \delta'_{i2}$, which also interprets the results in Fig. 5. Because natural surfaces are generally rough, the considered structure can explain the observed large values of V.

In Fig. 7 for the two-layer Sastrugi surface with $\varepsilon_1 = 1.8 + i6.0E - 4$ and $\varepsilon_2 = 1.3 + i3.3E - 4$, at the polar angle of $\theta = 55°$ and $\theta = 70°$, similarly, the vertical and horizontal brightness temperatures decrease more while the third Stokes parameter basically remains the same order with increase of the polar angle. It is also noted that the fourth

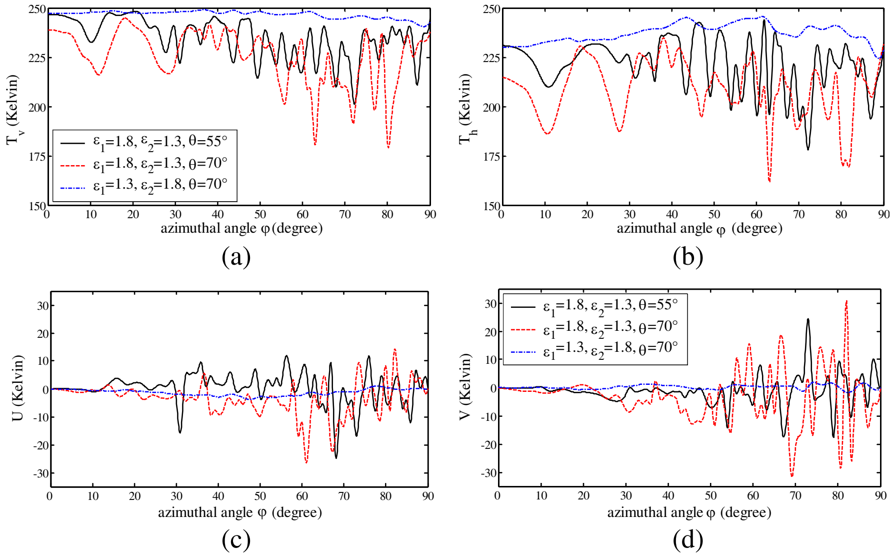

Figure 7. Four Stokes parameters versus azimuthal angle at freq = 10 GHz with $T_0 = 250\,\mathrm{K}$ from a two-layer Sastrugi surface with $d = 12.5\,\mathrm{cm}$. The solid line is at $\theta = 55^\circ$ while the dash line is at $\theta = 70^\circ$ both with $\varepsilon_1 = 1.8 + i6E-4$, $\varepsilon_2 = 1.3 + i3.3E-4$; the dash-dot line is at $\theta = 70^\circ$ with interchange of ε_1 and ε_2. (a) Vertical brightness, (b) horizontal brightness, (c) U brightness, and (d) V brightness.

Stokes parameter increases from $-18\,\mathrm{K} \sim 24\,\mathrm{K}$ to $-31\,\mathrm{K} \sim 31\,\mathrm{K}$. By interchanging of ε_1 and ε_2 even at a large polar angle of $\theta = 70^\circ$, the vertical and horizontal brightness temperatures decrease just a little and the third and fourth Stokes parameters are closer to zero due to no total internal reflection.

For the case of a single rough surface alone or a layered structure without total internal reflection due to $\varepsilon_1 < \varepsilon_2$, the angular trends of all four Stokes parameters are smooth and continuous except for some small artificial kinks and abruptions, which are imposed by effect of Floquet models due to periodic boundary condition. However, for the cases of layered structures with total internal reflection due to $\varepsilon_1 > \varepsilon_2$, the angular curves of all four components of Stokes vector become much more fluctuating. It is just because incident angles on the bottom interface change drastically relative to the critical angle although looking angles varying continuously, thus results in the total internal reflection taking place at different extents at different points of the bottom interface, accordingly, the angular behaviors of the four

Stokes parameters abrupt change, especially at large polar angle as shown in former Figures. Generally natural surfaces are not only rough but also random, so the random Sastrugi model, which is the future work, is an alternative choice to solve this problem by averaging over enough realizations.

4. CONCLUSION

In this paper, unlike $\varepsilon_1 < \varepsilon_2$ in Ref. [3], and different from flat face of the second interface in Ref. [5], a two-layer rough surface with $\varepsilon_1 > \varepsilon_2$ was used to simulate the four Stokes parameters. It is found that this new structure generates larger fourth Stokes parameter compared to those presented in Refs. [3] and [5]. Even for case of small slope surface with snow type permittivities of the three structures, only the rough-rough structure is able to produce large third and fourth Stokes parameters. The total internal reflection is the most critical factor to enlarge differences between polarizations, the larger surface slope make total reflection taking place easier. Medium with rough surface on both top and bottom interfaces is of more practical in reality, and thus the results reported in this paper are useful to interpret field measurements.

ACKNOWLEDGMENT

This work was supported in part by the Fundamental Research Funds for the Central Universities, in part by LIESMARS Special Research Funding and Open Fund of State Key Laboratory of Remote Sensing Science (Grant No. OFSLRSS201110).

REFERENCES

1. Veysoglu, M. E., H. A. Yueh, R. T. Shin, and J. A. Kong, "Polarimetric passive remote sensing of periodic surfaces," *Journal of Electromagnetic Waves and Applications*, Vol. 5, No. 3, 267–280, 1991.
2. Li, L., C. H. Chan, and L. Tsang, "Numerical simulation of conical diffraction of tapered electromagnetic waves from random rough surfaces and applications to passive remote sensing," *Radio Science*, Vol. 29, No. 3, 587–598, 1994.
3. Johnson, J. T., J. A. Kong, R. T. Shin, D. H. Staelin, K. O'Neill, and A. W. Lohanick, "Third stokes parameter emission from

a periodic water surface," *IEEE Trans. Geosci. Remote Sens.*, Vol. 31, No. 5, 1066–1080, Sep. 1993.

4. Li, L., P. Gaiser, M. R. Albert, D. G. Long, and E. M. Twarog, "WindSat passive microwave polarimetric signatures of the Greenland ice sheet," *IEEE Trans. Geosci. Remote Sens.*, Vol. 46, No. 9, 2622–2631, Sep. 2008.
5. Tsang, L., P. Xu, and K. S. Chen, "Third and fourth stokes parameters in polarimetric passive microwave remote sensing of rough surfaces over layered media," *Microwave Opt. Technol. Lett.*, Vol. 50, No. 12, 3063–3069, 2008.
6. Petit, R. (ed.), *Electromagnetic Theory of Gratings*, Vol. 22 of Topics in Current Physics, Springer-Verlag, Berlin, Heidelberg, New York, 1980.
7. Kuo, C. H. and M. Moghaddam, "Scattering from multilayer rough surfaces based on the extended boundary condition method and truncated singular value decomposition," *IEEE Trans. on Antennas Propag.*, Vol. 54, No. 10, 2917–2929, 2006.